

Crossover Between Weak Antilocalization and Weak Localization and Electron-Electron Interaction in Few-Layer WTe₂

Xurui Zhang¹, John M. Woods², Judy J. Cha², Xiaoyan Shi¹

¹*Department of Physics, The University of Texas at Dallas, Richardson, TX, USA*

²*Department of Mechanical Engineering and Materials Science, Yale University, New Haven, CT, USA*

We report electron transport studies in an encapsulated few-layer WTe₂ at low temperatures and high magnetic fields. The magnetoconductance reveals a temperature-induced crossover between weak antilocalization (WAL) and weak localization (WL) in quantum diffusive regime. We show that the crossover clearly manifests coexistence and competition among several characteristic lengths, including the dephasing length, the spin-flip length, and the mean free path. In addition, low temperature conductance increases logarithmically with the increase of temperature indicating an interplay of electron-electron interaction (EEI) and spin-orbit coupling (SOC). We demonstrate the existences and quantify the strengths of EEI and SOC which are considered to be responsible for gap opening in the quantum spin hall state in WTe₂ at the monolayer limit.

Keywords: Weak antilocalization, Quantum interference, Crossover, Electron-electron interaction, Spin-orbit coupling

Tungsten ditelluride (WTe₂), a layered transition metal dichalcogenide (TMD) crystal, has attracted a great deal of interests due to its unique electron transport properties. In the bulk form, WTe₂ has been predicted¹ and verified² to be the first type-II Weyl semimetal. However, the monolayer form of WTe₂ is either a quantum spin Hall insulator^{3,4} (QSHI) at low carrier density (n) or a superconductor⁵ at high n . For the QSHI state, a direct band gap emerges in bulk along with the topologically protected edge state. However, it is still unclear how a semimetallic band structure evolves into a gapped structure by reducing the thickness. It is proverbially believed that the band inversion happens in single-layer WTe₂, and a band gap is opened due to strong spin-orbit coupling (SOC)^{6,7}. However, another study verified that, instead of a full SOC-induced bulk band gap, a Coulomb gap induced by the electron-electron interaction (EEI) was observed⁸, which supports the observation of the quantized conduction of topological edge states. In addition, it is well known that EEI becomes stronger as n decreases, thus one can expect EEI should play an important role in the band gap opening. In order to have a better understanding of this mechanism, it is crucial to characterize both the SOC and EEI in WTe₂.

In weakly disordered electronic systems, the interaction between different scattering mechanisms gives rise to different transport behaviors. For example, the constructive quantum interference of the electrons moving through time-reversed scattering loops gives rise to a negative quantum correction to the conductance, which is so-called weak localization (WL)⁹⁻¹¹. On the contrary, the quantum interference induced by SOC gives rise to a positive correction known as the weak anti-localization (WAL)⁹⁻¹¹. Both WL and WAL can be suppressed by external magnetic field due to the time-reversal symmetry (TRS) breaking. In general, the quantum interference effect and thus its correction on electron conductance weakens as temperature (T) increases owing to enhanced decoherence mechanism. However, in some topological insulators, in spite of the existence of WAL effect with positive correction, the conductance decreases as the temperature is lowered¹²⁻¹⁷. This paradox can be solved by taking a strong EEI into account, which is known as the Altshuler–Aronov effect¹⁸. WTe₂ in low n region shows both a strong SOC and a strong EEI, thus this is a good platform to investigate SOC and EEI simultaneously in transport studies.

In this study, we investigate the SOC and EEI in few-layer WTe₂ by measuring both the temperature-dependent sheet conductance and magnetoconductance (MC). The strength of SOC can be quantified as the spin-flip length l_{so} , the distance travelled by an electron before its spin direction is changed by the scattering^{19,20}. The EEI can be characterized by the Coulomb screening factor F which is a measure of the screened Coulomb interaction^{21,22}. We also observe a temperature-induced crossover between WAL and WL. The mechanism of the crossover is clearly interpreted based on the relative change between spin-flip length l_{so} and dephasing length l_ϕ , the distance travelled by an electron within which it can maintain the phase coherence.

The thin WTe₂ flake, which was about 5 nm thick, was obtained by mechanical exfoliation of bulk WTe₂ crystals synthesized by chemical vapor transport²³. The exfoliated sample was encapsulated between two pieces of hexagonal Boron Nitride (hBN) thin flakes which were about 10 nm thick and transferred onto a silicon substrate with 285 nm SiO₂ coating on surface by dry transfer technique²⁴. Ultrathin WTe₂ flakes

are very easy to get oxidized in air^{5,25}. Hence the hBN flakes are necessary here to protect the sample from air. In addition, they provide a cleaner interface for WTe₂. The electron-beam lithography was used to make a pattern and the ohmic contacts were deposited by electron-beam evaporation of Pd/Au (10 nm/50 nm) followed by a lift-off process. Transport measurements down to 0.036 K were carried out in an Oxford dilution refrigerator. Both the longitudinal resistance R_{xx} and Hall resistance R_{xy} were measured simultaneously by using standard low frequency lock-in techniques. The corresponding four-probe measurement setup is shown in the inset of figure 1(a).

We first investigate the temperature dependence of sheet conductance, as shown in figure 1(a), at zero magnetic field ($H = 0$ T). We find two distinct regions divided by a critical temperature around $T_{\max} \approx 13.8$ K as shown in the inset of figure 1(a). Above this temperature, the resistance exhibits a typical metallic temperature dependence, which agrees with the expected semi-metal properties of bulk WTe₂. However, an up-turn occurs at T_{\max} , which indicates a tendency of weak localization. Fitting result shows that the low-temperature conductance is proportional to $\ln(T / T_{\max})$. Such relation has been observed in some topological materials¹²⁻¹⁷. In those experiments, a suppression of the conductance with decreasing temperature, like the case in this device, is observed along with weak antilocalization effect observed in magnetoconductance measurements which would enhance the conductance. Such a seeming paradox in topological insulator can be interpreted by the interplay of disorder and electron-electron interaction, which is known as the Altshuler–Aronov effect¹⁸. The correction from electron-electron interaction to the conductance would decrease logarithmically with decreasing temperature. The conductance enhancement from weak antilocalization could be overwhelmed which leads to an overall weak localization tendency. We further investigate the temperature dependent sheet conductance at various magnetic field as shown in figure 1(b). We find that the conductance at low temperature can be well fitted by equation $\sigma \sim \kappa \ln T$, where fitting parameter κ raises and saturates quickly as magnetic field increases (figure 1(b) inset). A detailed analysis will be provided in the latter part.

We also carry out magnetoconductance measurements to further investigate the weak antilocalization effect in perpendicular magnetic field. The magnetoconductance (MC) is defined as $\Delta\sigma(B) = \sigma(B) - \sigma(0)$, where $B = \mu_0 H$ is the effective magnetic field, at various constant temperatures, shown in figure 2(a). At high magnetic field, the sample exhibits quasi-parabolic MC which is common in WTe₂²⁵⁻³⁰. However, at low magnetic field, the parabolic MC doesn't dominate any more. At 0.036 K, a negative cusplike MC shows up at low field, which is a typical characteristic of WAL effect^{9,11}. With temperature increasing, the cusp in MC gradually broadens until 11 K, beyond which the MC becomes positive first then decreases again with the magnetic field increasing. The positive MC corresponds to the WL effect^{9,11}. This suggests that not only is there a temperature-dependent crossover between WL and WAL but it is very likely that WL and WAL coexist and compete. In order to better understand the characteristics of the sample, we carry out Hall measurements at different temperatures. The Hall resistance (R_{xy}) curves at different constant temperatures are shown in figure 2(b). These tight overlapping curves indicate that the carrier density is insensitive to temperature. The inset shows the R_{xy} curve at 0.036 K and the corresponding linear fit, which gives the sheet charge density $n = 6.25 \times 10^{13} \text{ cm}^{-2}$ and carrier mobility $\mu = 58.7 \text{ cm}^2 / \text{Vs}$. Therefore, this device is in a low n region and the charge transport is dominated by quantum diffusions. Furthermore, the mean free path is $l = \hbar k_F \mu / e = 7.6 \text{ nm}$, where \hbar is the reduced Plank constant, k_F is the Fermi wave vector, and e is the electron charge.

To analyze the temperature-dependent competition between WL and WAL, we introduce the two-component Hikami-Larkin-Nagaoka (HLN) theory for a 2D system^{9,10,31}

$$\Delta\sigma(B) = \sum_{i=0,1} \frac{\alpha_i e^2}{\pi \hbar} \left[\Psi \left(\frac{l_B^2}{l_{\phi_i}^2} + \frac{l_B^2}{l_i^2} + \frac{1}{2} \right) - \ln \left(\frac{l_B^2}{l_{\phi_i}^2} + \frac{l_B^2}{l_i^2} \right) \right], \quad (1)$$

where Ψ is the digamma function, α_0 and α_1 stand for the weights of WL and WAL respectively. In the limit of pure WAL, $\alpha_0 = 0$ and $\alpha_1 = -1/2$ for each band carrying a π Berry phase^{9,11,31-35}, while in the limit of pure WL, $\alpha_0 = 1$ and $\alpha_1 = 0$ for a usual 2D system and $\alpha_0 = 1/2$ and $\alpha_1 = 0$ for a

topological surface state^{9,11,31-35}. In the case of a coexistence of WL and WAL, α_0 and α_1 could take intermediate values. $l_B = \sqrt{\hbar / 4eB}$ is the magnetic length and all other characteristic lengths take the same form. l_{ϕ_i} is the corresponding dephasing length and l_i gives correction to l_{ϕ_i} . In WAL where SOC plays an important role, $l_i = l_{so}$, while in WL where SOC has nothing to do with, the l_i can be neglected. l_{so} is the spin-flip length, which describes the strength of SOC^{19,20,36}. Of course there are some other mechanisms that can be included in l_i , like magnetic scattering which needs to be discussed in some magnetically doped samples^{34,37-41}, but this does not apply to our situation. In addition, considering the particularity of WTe₂ in which the intrinsic quasi-parabolic positive magnetoresistance (MR) originating from carrier compensation cannot be ignored, we introduce a quadratic term as the background²⁵⁻³⁰, such that

$$\Delta\sigma(B)_{FIT} = \Delta\sigma(B) + cB^2 \quad (2)$$

where c is a constant that depends on the measurement temperature. To all the temperature-dependent $\Delta\sigma(B)$ traces, Eq. (2) fits the data in low-field region (-2 T to 2 T) very well. For clarity, the fits are shown in Fig. 3(a) and (b) for WAL-dominant and WL-dominant regimes, respectively. The coincidence of the fitting curves and the experimental data validates the perfect applicability of the HLN model.

Figure 4(a) shows the evolution of $|\alpha_0|$ ($\alpha_0 > 0$) and $|\alpha_1|$ ($\alpha_1 < 0$), obtained from the two-component HLN fitting, as a function of temperature. From 0.036 K to 25 K, α_1 changes slowly from -0.5 to -0.44 while α_0 increases drastically from 0.16 to 0.5. The half integer values of α_0 and α_1 indicate the existence of the topological surface state in WTe₂ ultrathin film. It's worth mentioning that the very small change in α_1 and dramatic change in α_0 indicate that WL is much more sensitive to the temperature than WAL.

In order to investigate the mechanism of the crossover and competition between WL and WAL, we further

examine the changes in several characteristic lengths with temperature. Temperature dependence of the dephasing lengths for WL (l_{ϕ_0}) and WAL (l_{ϕ_1}) and the spin-flip length (l_{so}) are shown in Fig. 4(b). The rapid reduction of the dephasing lengths indicates that the inelastic scattering in this sample is enhanced drastically as T increases. It is also of note that the dephasing lengths are much larger than the film thickness and the mean free path ($l = 7.6$ nm) even at high temperature, which confirms the transport measurements are indeed in the 2D quantum diffusion regime. Power-law fits to the dephasing lengths in logarithmic coordinate (inset of Fig. 4(b)) give $l_{\phi_0} \sim T^{-0.25}$ for WL and $l_{\phi_1} \sim T^{-0.23}$ for WAL. The almost identical temperature dependence is expected since the electrons participating in WL and WAL pass through the same or similar TRS loops and undergo the same inelastic scattering which depends on the temperature only. The only difference is that the electrons participating in WAL undergo frequent spin flips which generate a π Berry phase after moving through a scattering loop. This π Berry phase is responsible for the destructive quantum interference that suppresses the back scattering and enhances the conductance, leading to the WAL. In present case, the effective exponent of temperature p is ~ 0.5 in $l_{\phi} \sim T^{-p/2}$ which is considerably lower than that theoretically expected p exponent ($p = 1$) for the Nyquist electron-electron scattering process in 2D^{42,43}. However, a similar $p \sim 0.5$ has been observed in topological insulator Bi₂Se₃ micro-flakes, where EEI plays important roles^{14,44,45}. Based on the temperature dependence of conductance and the power law dependence of l_{ϕ} , we believe that there exist additional electron dephasing processes which are noticeable over the experimental temperature range in our sample as well.

Now we focus on the mechanism of the crossover between WL and WAL. Since the π Berry phase induced by SOC is the key to determining whether a sample presents WL or WAL, we plot l_{so} , which reflects the strength of SOC and the band topology, as a function of temperature in Fig. 4(b). We find that l_{so} can be well described with power-law fit ($l_{so} \sim T^{-0.14}$) below a characteristic temperature $T_{so} \sim 11$ K (Fig. 4(b) inset), which is exactly the WAL dominant regime. Beyond T_{so} , the l_{so} decreases

even faster and deviates from the power-law decay as temperature increases. In contrast, both \mathcal{L}_{ϕ_0} and \mathcal{L}_{ϕ_1} maintain the power-law decay up to 25 K, which indicates the quantum interference can survive in a much higher T than SOC. In high T , where \mathcal{L}_{so} approaches to and even smaller than the mean free path, the symmetry class changes from symplectic to orthogonal^{46,10} and thus the quantum interference correction will crossover from WAL to WL as temperature increases. In a topological insulating system, the effect of quantum interference can be characterized by two time scales³⁶: the dephasing time τ_ϕ and the spin-flip time τ_{so} with the relation $\mathcal{L}_j^2 = D\tau_j$ where \mathcal{L}_j can be \mathcal{L}_ϕ or \mathcal{L}_{so} , and D is the electron diffusion coefficient. Let's evaluate the characteristic lengths and related time qualitatively in both WL and WAL processes. In the regime $\tau_\phi \gg \tau_{so}$, the spin of the electron undergoes very frequent flips which makes destructive quantum interference between the TRS scattering loops, leading to WAL. In the regime where τ_ϕ is comparable to τ_{so} or $\tau_\phi < \tau_{so}$, the spin orientation is not that frequently changed by the scattering. In such case, constructive quantum interference occurs as a WL feature. In the intermediate regime where $\tau_\phi > \tau_{so}$, there will be a situation where WL and WAL may coexist. since τ_ϕ and τ_{so} could vary with temperature, this variation signifies a crossover between WAL and WL. In present sample, we have $\mathcal{L}_\phi \approx 175$ nm (taken from \mathcal{L}_{ϕ_1} in WAL dominant regime), $\mathcal{L}_{so} \approx 24$ nm $\gg \mathcal{L}$ at 0.036 K and $\mathcal{L}_\phi \approx 30$ nm (taken from \mathcal{L}_{ϕ_0} in WL dominant regime), $\mathcal{L}_{so} \approx 7$ nm $\approx \mathcal{L}$ at 25 K. These fitting results give $\tau_\phi / \tau_{so} \approx 53$ at 0.036 K and $\tau_\phi / \tau_{so} \approx 18$ at 25 K. We conclude that our sample is in an ambiguous state between WAL regime in which $\tau_\phi \gg \tau_{so}$ and intermediate regime where $\tau_\phi > \tau_{so}$ at 0.036 K. With the temperature increasing, the difference between τ_ϕ and τ_{so} is narrowing and our sample enters into the intermediate regime, giving rise to the co-existence of WL and WAL. This sample never goes into pure WL regime which requires $\tau_\phi < \tau_{so}$ and presents a sharply downward cusplike MC.

In previous discussion of MC, we don't take EEI into consideration. Although the role of EEI dominates in

temperature dependence of conductance, MC due to EEI is at least one order smaller than that due to quantum interference in perpendicular magnetic field^{11,13,16,17}. The EEI affects MC indirectly via the Zeeman

splitting. The correction to the conductance is $\Delta\sigma_{EEI}(B) = \frac{e^2}{\pi h} \frac{\tilde{F}^\sigma}{2} g_2\left(\frac{E_z}{k_B T}\right)$, where \tilde{F}^σ is the Coulomb

screening factor, g_2 is an integral function, and E_z is the Zeeman energy^{13,17}. In the regime where EEI are important, the Zeeman contribution could be strongly suppressed by SOC. Theories^{47,48} and experiments⁴⁹ on other materials have unambiguously shown that strong SOC can diminish and even entirely suppress the Zeeman-split term in the diffusion channel¹³.

In contrast, in analysis of temperature-dependent sheet conductance, it's necessary to consider both EEI and quantum interference. The quantum correction to the conductance resulting from WAL at zero magnetic field is given as^{12,50,51}

$$\Delta\sigma_{QI}(T) = \alpha p \frac{e^2}{\pi h} \ln\left(\frac{T}{T_{QI}}\right) \quad (3)$$

where α is exactly the same parameter discussed in HLN model and p is the exponent in the power-law fit of dephasing lengths. T_{QI} is a characteristic temperature at which the quantum correction vanishes. The correction to the conductance coming from EEI is given by^{11,12,14,16,17}

$$\Delta\sigma_{EEI}(T) = \frac{e^2}{\pi h} \left(1 - \frac{3}{4} F\right) \ln\left(\frac{T}{T_{EEI}}\right) \quad (4)$$

where F is the simplified Coulomb screening factor, which is not critical to be distinguished with \tilde{F}^σ in most experiments^{21,22}. T_{EEI} is the characteristic temperature for the EEI effect. In most experiments, T_{QI} and T_{EEI} are considered to be the same and to be the turning point in the temperature-dependent conductance, which is $T_{\max} = 13.8$ K in our case. Having summed the WAL and EEI contributions together, we got the slope to be $\alpha p + \left(1 - \frac{3}{4} F\right) = 0.53$ at 0 T, obtained from the fitting $\Delta\sigma(T) \propto \ln(T/T_{\max})$ shown as the black dashed line in Fig 1(a). Since the sample is in WAL dominant

regime below 13.8 K, we only take the weight of WAL, α_1 , which is almost unchanged between -0.5 and -0.47. Having $p = 0.46$ obtained from the aforementioned fit, we got the Coulomb screening factor $0.32 \leq F \leq 0.34$. This F value is in good agreement with the theory that F is between -1 and 1 with $F \rightarrow 1$ in the limit of complete screening (good metal) and $F \rightarrow 0$ in the limit of no screening (bad conductor)²². The fitting slopes at various magnetic fields shown in the inset of figure 1(b) agree well with Chen's results¹³, which is theoretically verified to be a single topological surface channel¹¹. Since the quantum interference is strongly suppressed at high magnetic field, the slope at 12 T should be totally attributed to EEI. By only fitting with equation (4), we get the Coulomb screening factor F to be 0.32 which agrees with the estimated value at 0 T. This also confirms our analysis of MC. In some topological materials, people got negative F , which might be related to strong electron-phonon coupling^{21,52} or contribution from bulk state¹². Even though strong SOC is confirmed in this sample, we still get a reasonable value of F in the expected range which is in good agreement with theory. This agreement strongly indicates the very first observation of electron-electron interaction in few-layer WTe₂ in transport studies. Similar existence of EEI has been confirmed in monolayer samples⁸. In monolayer WTe₂, the opening of the Coulomb gap induced by EEI can diminish the bulk state and support the quantized conduction of topological edge states⁸. Unlike the monolayer samples, this few-layer WTe₂ device shows both a semi-metallic $\sigma(T)$ at high T as expected for bulk and an EEI induced $\ln(T)$ behavior at low T as expected for monolayer. This temperature-tuned crossover in the conductance bridges the conductance in two extreme cases and provides a uniform picture of understanding in the transport behavior in WTe₂.

In conclusion, we have investigated the quantum interference and electron-electron interaction in encapsulated few-layer WTe₂. At low temperatures, a clear WAL to WL crossover revealed a manifestation of coexistence and competition among several characteristic lengths. With increasing either temperature or magnetic field, the topologic non-trivial transport fades out and a related Coulomb gap closes. In this process, both SOC and EEI play important roles. In addition, quantum interference, and thus TRS, can survive in a much higher temperature, which makes WTe₂ a promising platform for further investigation in the interplay of SOC and band topology. As an intermediate form between the monolayer and the bulk

limits, few-layer devices could behave as either limit by simple tuning of temperatures. This unique feature may enable new spintronic applications.

Acknowledgement

This work was supported by UT Dallas research enhancement fund. Synthesis of WTe₂ crystals was supported by DOE BES Award No. DE-SC0014476.

References:

1. Soluyanov, A. A., Gresch, D., Wang, Z., Wu, Q., Troyer, M., Dai, X., & Bernevig, B. A. Type-II Weyl semimetals. *Nature* **527**, 495–498 (2015).
2. Li, P., Wen, Y., He, X., Zhang, Q., Xia, C., Yu, Z.-M., Yang, S. A., Zhu, Z., Alshareef, H. N., & Zhang, X.-X. Evidence for topological type-II Weyl semimetal WTe2. *Nat. Commun.* **8**, 2150 (2017).
3. Wu, S., Fatemi, V., Gibson, Q. D., Watanabe, K., Taniguchi, T., Cava, R. J., & Jarillo-Herrero, P. Observation of the quantum spin Hall effect up to 100 kelvin in a monolayer crystal. *Science (80-.)* **359**, 76 LP – 79 (2018).
4. Qian, X., Liu, J., Fu, L., & Li, J. Quantum spin Hall effect in two-dimensional transition metal dichalcogenides. *Science (80-.)* **346**, 1344 LP – 1347 (2014).
5. Fatemi, V., Wu, S., Cao, Y., Bretheau, L., Gibson, Q. D., Watanabe, K., Taniguchi, T., Cava, R. J., & Jarillo-Herrero, P. Electrically tunable low-density superconductivity in a monolayer topological insulator. *Science (80-.)* **362**, 926 LP – 929 (2018).
6. Jia, Z.-Y., Song, Y.-H., Li, X.-B., Ran, K., Lu, P., Zheng, H.-J., Zhu, X.-Y., Shi, Z.-Q., Sun, J., Wen, J., Xing, D., & Li, S.-C. Direct visualization of a two-dimensional topological insulator in the single-layer 1T'-WTe2. *Phys. Rev. B* **96**, 41108 (2017).
7. Tang, S., Zhang, C., Wong, D., Pedramrazi, Z., Tsai, H.-Z., Jia, C., Moritz, B., Claassen, M., Ryu, H., Kahn, S., Jiang, J., Yan, H., Hashimoto, M., Lu, D., Moore, R. G., Hwang, C.-C., Hwang, C., Hussain, Z., Chen, Y. *et al.* Quantum spin Hall state in monolayer 1T'-WTe2. *Nat. Phys.* **13**, 683–687 (2017).
8. Song, Y.-H., Jia, Z.-Y., Zhang, D., Zhu, X.-Y., Shi, Z.-Q., Wang, H., Zhu, L., Yuan, Q.-Q., Zhang, H., Xing, D.-Y., & Li, S.-C. Observation of Coulomb gap in the quantum spin Hall candidate single-layer 1T'-WTe2. *Nat. Commun.* **9**, 4071 (2018).
9. Lu, H. Z., Shi, J., & Shen, S. Q. Competition between weak localization and antilocalization in topological surface states. *Phys. Rev. Lett.* **107**, 1–5 (2011).
10. Hikami, S., Larkin, A. I., & Nagaoka, Y. Spin-Orbit Interaction and Magnetoresistance in the Two Dimensional Random System. *Prog. Theor. Phys.* **63**, 707–710 (1980).
11. Lu, H.-Z. & Shen, S.-Q. Finite-Temperature Conductivity and Magnetoconductivity of Topological Insulators. *Phys. Rev. Lett.* **112**, 146601 (2014).
12. Takagaki, Y., Jenichen, B., Jahn, U., Ramsteiner, M., & Friedland, K.-J. Weak antilocalization and electron-electron interaction effects in Cu-doped Bi2Se3 films. *Phys. Rev. B* **85**, 115314 (2012).
13. Chen, J., He, X. Y., Wu, K. H., Ji, Z. Q., Lu, L., Shi, J. R., Smet, J. H., & Li, Y. Q. Tunable surface conductivity in Bi2Se3 revealed in diffusive electron transport. *Phys. Rev. B* **83**, 241304 (2011).
14. Chiu, S.-P. & Lin, J.-J. Weak antilocalization in topological insulator Bi2Se3 microflakes. *Phys. Rev. B* **87**, 35122 (2013).
15. Roy, A., Guchhait, S., Sonde, S., Dey, R., Pramanik, T., Rai, A., Mowa, H. C. P., Colombo, L., & Banerjee, S. K. Two-dimensional weak anti-localization in Bi2Te3 thin film grown on Si(111)-(7 × 7) surface by molecular beam epitaxy. *Appl. Phys. Lett.* **102**, 163118 (2013).
16. Wang, J., DaSilva, A. M., Chang, C.-Z., He, K., Jain, J. K., Samarth, N., Ma, X.-C., Xue, Q.-K., & Chan, M. H. W. Evidence for electron-electron interaction in topological insulator thin films. *Phys. Rev. B* **83**, 245438 (2011).
17. Liu, M., Chang, C.-Z., Zhang, Z., Zhang, Y., Ruan, W., He, K., Wang, L., Chen, X., Jia, J.-F., Zhang, S.-C., Xue, Q.-K., Ma, X., & Wang, Y. Electron interaction-driven insulating ground state in Bi2Se3 ological insulators in the two-

- dimensional limit. *Phys. Rev. B* **83**, 165440 (2011).
- 18. Altshuler, B. L., Aronov, A. G., & Lee, P. A. Interaction effects in disordered fermi systems in two dimensions. *Phys. Rev. Lett.* **44**, 1288–1291 (1980).
 - 19. Meng, M., Huang, S., Tan, C., Wu, J., Jing, Y., Peng, H., & Xu, H. Q. Strong spin–orbit interaction and magnetotransport in semiconductor Bi₂O₂Se nanoplates. *Nanoscale* **10**, 2704–2710 (2018).
 - 20. Herling, F., Morrison, C., Knox, C. S., Zhang, S., Newell, O., Myronov, M., Linfield, E. H., & Marrows, C. H. Spin–orbit interaction in InAs/GaSb heterostructures quantified by weak antilocalization. *Phys. Rev. B* **95**, 155307 (2017).
 - 21. Wu, C. Y., Jian, W. B., & Lin, J. J. Phonon-induced electron–electron interaction in disordered superconductors. *Phys. Rev. B* **52**, 15479–15484 (1995).
 - 22. Lin, J. J., Hsu, S. Y., Lue, J. C., & Sheng, P. J. Spin–orbit scattering effect on electron–electron interactions in disordered metals. *J. Phys. Chem. Solids* **62**, 1813–1818 (2001).
 - 23. Woods, J. M., Shen, J., Kumaravadivel, P., Pang, Y., Xie, Y., Pan, G. A., Li, M., Altman, E. I., Lu, L., & Cha, J. J. Suppression of Magnetoresistance in Thin WTe₂ Flakes by Surface Oxidation. *ACS Appl. Mater. Interfaces* **9**, 23175–23180 (2017).
 - 24. Castellanos-Gomez, A., Buscema, M., Molenaar, R., Singh, V., Janssen, L., Van Der Zant, H. S. J., & Steele, G. A. Deterministic transfer of two-dimensional materials by all-dry viscoelastic stamping. *2D Mater.* **1**, 1–34 (2014).
 - 25. Wang, L., Gutiérrez-Lezama, I., Barreteau, C., Ubrig, N., Giannini, E., & Morpurgo, A. F. Tuning magnetotransport in a compensated semimetal at the atomic scale. *Nat. Commun.* **6**, 8892 (2015).
 - 26. Ali, M. N., Xiong, J., Flynn, S., Tao, J., Gibson, Q. D., Schoop, L. M., Liang, T., Haldolaarachchige, N., Hirschberger, M., Ong, N. P., & Cava, R. J. Large, non-saturating magnetoresistance in WTe₂. *Nature* **514**, 205–208 (2014).
 - 27. Cai, P. L., Hu, J., He, L. P., Pan, J., Hong, X. C., Zhang, Z., Zhang, J., Wei, J., Mao, Z. Q., & Li, S. Y. Drastic Pressure Effect on the Extremely Large Magnetoresistance in WTe₂: Quantum Oscillation Study. *Phys. Rev. Lett.* **115**, 57202 (2015).
 - 28. Fatemi, V., Gibson, Q. D., Watanabe, K., Taniguchi, T., Cava, R. J., & Jarillo-Herrero, P. Magnetoresistance and quantum oscillations of an electrostatically tuned semimetal-to-metal transition in ultrathin \$\mathrm{WTe}_2\$. *Phys. Rev. B* **95**, 41410 (2017).
 - 29. Woods, J. M., Shen, J., Kumaravadivel, P., Pang, Y., Xie, Y., Pan, G. A., Li, M., Altman, E. I., Lu, L., & Cha, J. J. Suppression of Magnetoresistance in Thin WTe₂ Flakes by Surface Oxidation. *ACS Appl. Mater. Interfaces* **9**, 23175–23180 (2017).
 - 30. Jiang, J., Tang, F., Pan, X. C., Liu, H. M., Niu, X. H., Wang, Y. X., Xu, D. F., Yang, H. F., Xie, B. P., Song, F. Q., Dudin, P., Kim, T. K., Hoesch, M., Das, P. K., Vobornik, I., Wan, X. G., & Feng, D. L. Signature of Strong Spin-Orbital Coupling in the Large Nonsaturating Magnetoresistance Material WTe₂. *Phys. Rev. Lett.* **115**, 166601 (2015).
 - 31. Newton, P. J., Mansell, R., Holmes, S. N., Myronov, M., & Barnes, C. H. W. Weak localization and weak antilocalization in doped germanium epilayers. *Appl. Phys. Lett.* **110**, (2017).
 - 32. Lang, M., He, L., Kou, X., Upadhyaya, P., Fan, Y., Chu, H., Jiang, Y., Bardarson, J. H., Jiang, W., Choi, E. S., Wang, Y., Yeh, N.-C., Moore, J., & Wang, K. L. Competing Weak Localization and Weak Antilocalization in Ultrathin Topological Insulators. *Nano Lett.* **13**, 48–53 (2013).
 - 33. Wang, W.-H., Lyu, S.-R., Heredia, E., Liu, S.-H., Jiang, P., Liao, P.-Y., Chang, T.-C., & Chen, H.-M. Competing weak localization and weak antilocalization in amorphous indium–gallium–zinc-oxide thin-film transistors. *Appl. Phys. Lett.* **110**, 22106 (2017).

34. Liu, M., Zhang, J., Chang, C., Zhang, Z., Feng, X., Li, K., He, K., Wang, L., Chen, X., Dai, X., Fang, Z., Xue, Q., Ma, X., & Wang, Y. Crossover between Weak Antilocalization and Weak Localization in a Magnetically Doped Topological Insulator. *Phys. Rev. Lett.* **108**, 036805 (2012).
35. Choo, S. M., Lee, K. J., Park, S. M., Yoon, J. B., Park, G. S., You, C.-Y., & Jung, M. H. Crossover between weak anti-localization and weak localization by Co doping and annealing in gapless PbPdO₂ and spin gapless Co-doped PbPdO₂. *Appl. Phys. Lett.* **106**, 172404 (2015).
36. Wang, H., Liu, H., Chang, C.-Z., Zuo, H., Zhao, Y., Sun, Y., Xia, Z., He, K., Ma, X., Xie, X. C., Xue, Q.-K., & Wang, J. Crossover between Weak Antilocalization and Weak Localization of Bulk States in Ultrathin Bi₂Se₃ Films. *Sci. Rep.* **4**, 5817 (2014).
37. Wray, L. A., Xu, S.-Y., Xia, Y., Hsieh, D., Fedorov, A. V., Hor, Y. S., Cava, R. J., Bansil, A., Lin, H., & Hasan, M. Z. A topological insulator surface under strong Coulomb, magnetic and disorder perturbations. *Nat. Phys.* **7**, 32–37 (2011).
38. Hor, Y. S., Roushan, P., Beidenkopf, H., Seo, J., Qu, D., Checkelsky, J. G., Wray, L. A., Hsieh, D., Xia, Y., Xu, S.-Y., Qian, D., Hasan, M. Z., Ong, N. P., Yazdani, A., & Cava, R. J. Development of ferromagnetism in the doped topological insulator Bi₂–xMn_xTe₃. *Phys. Rev. B* **81**, 195203 (2010).
39. Zheng, G., Wang, N., Yang, J., Wang, W., Du, H., Ning, W., Yang, Z., Lu, H.-Z., Zhang, Y., & Tian, M. Weak localization effect in topological insulator micro flakes grown on insulating ferrimagnet BaFe₁₂O₁₉. *Sci. Rep.* **6**, 21334 (2016).
40. Yang, Q. I., Dolev, M., Zhang, L., Zhao, J., Fried, A. D., Schemm, E., Liu, M., Palevski, A., Marshall, A. F., Risbud, S. H., & Kapitulnik, A. Emerging weak localization effects on a topological insulator--insulating ferromagnet (Bi₂Se₃-EuS) interface. *Phys. Rev. B* **88**, 81407 (2013).
41. Zhang, D., Richardella, A., RENCH, D. W., Xu, S.-Y., Kandala, A., Flanagan, T. C., Beidenkopf, H., Yeats, A. L., Buckley, B. B., Klimov, P. V., Awschalom, D. D., Yazdani, A., Schiffer, P., Hasan, M. Z., & Samarth, N. Interplay between ferromagnetism, surface states, and quantum corrections in a magnetically doped topological insulator. *Phys. Rev. B* **86**, 205127 (2012).
42. Wu, C.-Y., Lin, B.-T., Zhang, Y.-J., Li, Z.-Q., & Lin, J.-J. Electron dephasing in homogeneous and inhomogeneous indium tin oxide thin films. *Phys. Rev. B* **85**, 104204 (2012).
43. Altshuler, B. L., Aronov, A. G., & Khmel'nitsky, D. E. Effects of electron-electron collisions with small energy transfers on quantum localisation. *J. Phys. C Solid State Phys.* **15**, 7367–7386 (1982).
44. Huang, S. M., Lee, T. C., Akimoto, H., Kono, K., & Lin, J. J. Observation of Strong Electron Dephasing in Highly Disordered $\{\mathrm{Cu}\}_{93}\{\mathrm{Ge}\}_{4}\{\mathrm{Au}\}_3$ Thin Films. *Phys. Rev. Lett.* **99**, 46601 (2007).
45. Lin, J. J. & Bird, J. P. Recent experimental studies of electron dephasing in metal and semiconductor mesoscopic structures. *J. Phys. Condens. Matter* **14**, R501–R596 (2002).
46. Dyson, F. J. Statistical Theory of the Energy Levels of Complex Systems. I. *J. Math. Phys.* **3**, 140–156 (1962).
47. Lee, P. A. & Ramakrishnan, T. V. Disordered electronic systems. *Rev. Mod. Phys.* **57**, 287–337 (1985).
48. Altshuler, B. L., Aronov, A. G., & Zuzin, A. Y. Spin relaxation and interaction effects in the disordered conductors. *Solid State Commun.* **44**, 137–139 (1982).
49. Sahnoun, A., Ström-Olsen, J. O., & Fischer, H. E. Influence of spin-orbit scattering on the magnetoresistance due to enhanced electron-electron interactions. *Phys. Rev. B* **46**, 10035–10040 (1992).
50. McCann, E., Kechedzhi, K., Fal'ko, V. I., Suzuura, H., Ando, T., & Altshuler, B. L. Weak-Localization

- Magnetoresistance and Valley Symmetry in Graphene. *Phys. Rev. Lett.* **97**, 146805 (2006).
51. Tkachov, G. & Hankiewicz, E. M. Weak antilocalization in HgTe quantum wells and topological surface states: Massive versus massless Dirac fermions. *Phys. Rev. B* **84**, 35444 (2011).
52. Giraud, S. & Egger, R. Electron-phonon scattering in topological insulators. *Phys. Rev. B* **83**, 245322 (2011).

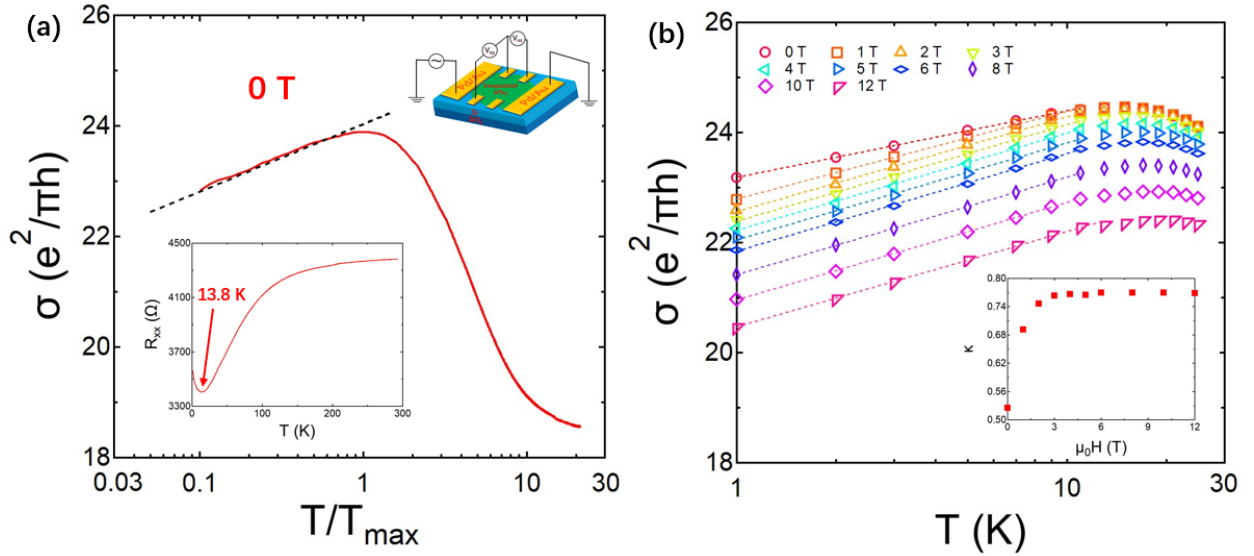


Figure 1. (a) Temperature dependence of sheet conductance at zero magnetic field (red solid line). The black dashed line is the logarithmic fit at low temperature regime ($T < 13.8$ K). Insets show the temperature-dependent resistance (lower left) and a schematic diagram of the measurement setup (upper right). The red arrow marks the up-turn at 13.8 K. (b) Temperature dependence of sheet conductance (hollow symbols) at various magnetic fields. The dashed lines are the logarithmic fits at low temperature regime. Inset shows the slopes κ as a function of magnetic field.

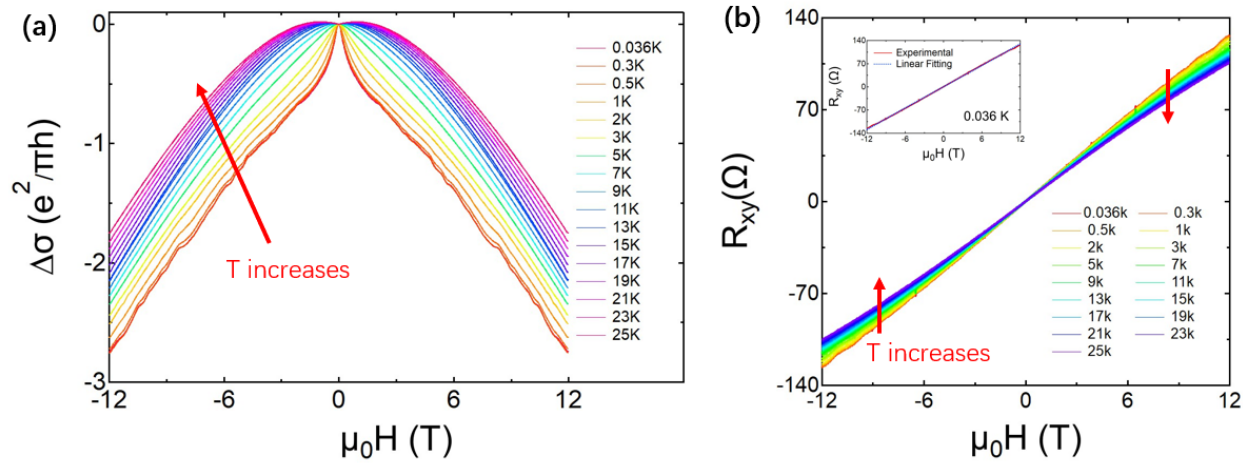


Figure 2. (a) Temperature dependence of the magnetoconductance, defined as $\Delta\sigma(H) = \sigma(H) - \sigma(0)$, in unit of $e^2/\pi\hbar$. (b) Temperature dependence of the Hall resistance. Inset is the linear fit to the Hall resistance at 0.036 K which gives $n = 6.25 \times 10^{13} \text{ cm}^{-2}$. Red arrows in both panels denote the direction of increasing temperature.

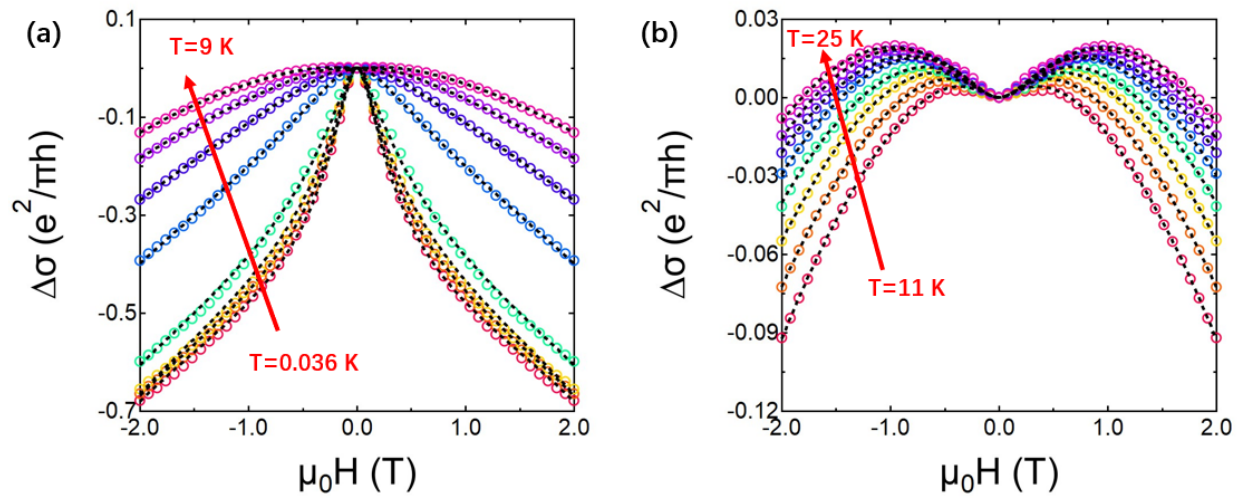


Figure 3. Magnetoconductance $\Delta\sigma(H)$ at (a) low temperatures (0.036 K to 9 K) and (b) high temperatures (11 K to 25 K). Hollow circles and dashed lines are experimental data and two-component HLN fits, respectively. Red arrows indicate the direction of increasing temperature.

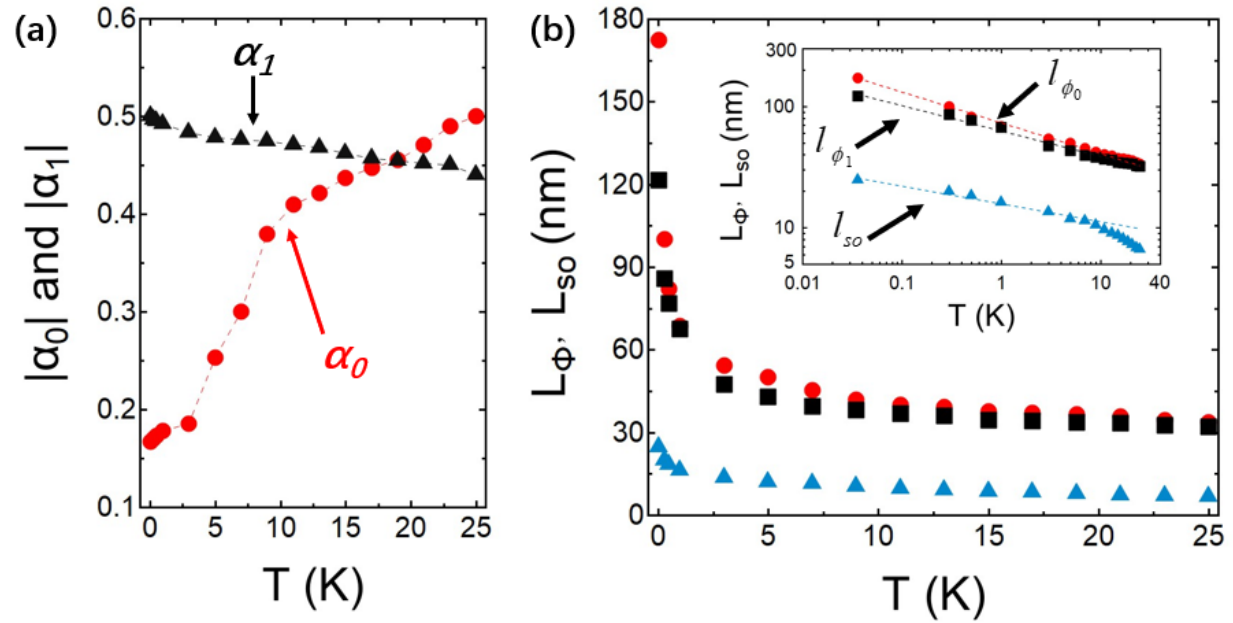


Figure 4. Temperature dependence of (a) $|\alpha_0|$ and $|\alpha_1|$, and (b) L_{ϕ_0} and L_{ϕ_1} . Inset of (b): the same set of data, as in the main plot, are shown in log-log plot. Dashed lines are the power-law fits.